Detection of irrigated and rainfed crops in temperate areas using Sentinel-1 and Sentinel-2 time series

Yann Pageot, Frédéric Baup, Jordi Inglada, Nicolas Baghdadi, Valérie Demarez

To cite this version:

Yann Pageot, Frédéric Baup, Jordi Inglada, Nicolas Baghdadi, Valérie Demarez. Detection of irrigated and rainfed crops in temperate areas using Sentinel-1 and Sentinel-2 time series. Remote Sensing, 2020, Irrigation Mapping Using Satellite Remote Sensing, 12 (18), pp.3044. ⟨10.3390/rs12183044⟩. ⟨hal-02952478⟩

HAL Id: hal-02952478
https://hal.inrae.fr/hal-02952478v1

Submitted on 29 Sep 2020

remote sensing

MDPI

Article

Detection of Irrigated and Rainfed Crops in Temperate Areas Using Sentinel-1 and Sentinel-2 Time Series

Yann Pageot [1,*], **Frédéric Baup** [1], **Jordi Inglada** [1], **Nicolas Baghdadi** [2] and **Valérie Demarez** [1]

[1] Centre d'Etudes Spatiales de la Biosphère, Université de Toulouse, CNES/CNRS/IRD/INRA/UPS, 18 av. Edouard Belin, bpi 2801, CEDEX 9 31401 Toulouse, France; frederic.baup@iut-tlse3.fr (F.B.); jordi.inglada@cesbio.eu (J.I.); valerie.demarez@cesbio.cnes.fr (V.D.)

[2] TETIS, INRAE, University of Montpellier, 500 rue François Breton, CEDEX 5 34093 Montpellier, France; nicolas.baghdadi@teledetection.fr

* Correspondence: yann.pageot@cesbio.cnes.fr

Received: 10 August 2020; Accepted: 15 September 2020; Published: 17 September 2020

Abstract: The detection of irrigated areas by means of remote sensing is essential to improve agricultural water resource management. Currently, data from the Sentinel constellation offer new possibilities for mapping irrigated areas at the plot scale. Until now, few studies have used Sentinel-1 (S1) and Sentinel-2 (S2) data to provide approaches for mapping irrigated plots in temperate areas. This study proposes a method for detecting irrigated and rainfed plots in a temperate area (southwestern France) jointly using optical (Sentinel-2), radar (Sentinel-1) and meteorological (SAFRAN) time series, through a classification algorithm. Monthly cumulative indices calculated from these satellite data were used in a Random Forest classifier. Two data years have been used, with different meteorological characteristics, allowing the performance of the method to be analysed under different climatic conditions. The combined use of the whole cumulative data (radar, optical and weather) improves the irrigated crop classifications (Overall Accuary (OA) ≈ 0.7) compared to the classifications obtained using each data separately (OA < 0.5). The use of monthly cumulative rainfall allows a significant improvement of the Fscore of irrigated and rainfed classes. Our study also reveals that the use of cumulative monthly indices leads to performances similar to those of the use of 10-day images while considerably reducing computational resources.

Keywords: irrigation; summer crops; random forest; high spatial and temporal resolution; temperate areas

1. Introduction

Human activities have an impact on the different components of the hydrosphere, and 80% of the world's population is now facing water shortages that will worsen with global warming [1]. Faced with this emergency situation, it is necessary to develop adaptation strategies to allow access to water resources for the entire population and to maintain agricultural activity. One of the adaptation strategies that has been favoured is irrigation. FAO estimates that 80% of the food needs in 2025 will be covered by irrigated agriculture [2] and more than 324 million hectares are equipped for irrigation in the world [3]. However, the use of irrigation has led to conflicts on water uses that are likely to worsen in a context of climate change. Rational and collective management of water resources has therefore become crucial. To achieve this objective, explicit information on agricultural practices and on the amount of water needed for crops over large areas is needed [4]. In this context, remote sensing observation could play an essential role. Many studies have proposed methodologies based on remote sensing images to derive useful indicators for water management [4–6]. Many of them have used multispectral and multi-temporal remote sensing images to map irrigated areas [7–14], demonstrating the high potential of remote sensing data. However, most of these studies are conducted in semi-arid areas [15–23]. Very little research is carried out in temperate areas, which also suffer from water scarcity. In France, for example, each year, about twenty departments (Nomenclature of Territorial Units for Statistics level 3) apply water restrictions. This number increases in the driest years: 73 departments (among 101) in the summer of 2019. In temperate areas, the detection of irrigated plots is difficult because of the the smaller differences in observed phenology between irrigated and rainfed crops compared to what is observed in semi-arid zones [24,25]. This smaller differences is related to local agricultural practices and pedoclimatic conditions.

The launch of the Sentinel constellation gives a new opportunity for the mapping of land cover and agricultural practices [26,27]. Numerous studies have shown that using temporally dense optical time series can improve crop mapping over different climates [28–32]. Vogels et al. [33] used a new approach to map irrigated areas in the Horn of Africa: a Sentinel 2 times series. However, as optical imagery is affected by cloud cover, the performance of the crop mapping with such data can be reduced in some cases, particularly for temperate or tropical areas [33] . Other recent studies [34–39] have shown that the joint use of optical and radar data improves the robustness of the mapping methods [21,35,37]. Nevertheless, all the studies mentioned above deal with the mapping of irrigated areas in arid or semi-arid climatic areas. There are few works on mapping irrigated crops in temperate areas with high spatial and temporal resolution. Demarez et al. [36] demonstrated than combining high spatial and temporal optical imagery (Landsat-8) and SAR (Synthetic Aperture Radar) imagery (Sentinel-1) allows to improve the detection of irrigated areas in the southwest of France. However, in this study the main limiting factor was the temporal resolution of the Landsat-8 images.

In this work, we propose a new methodology for distinguishing irrigated and rainfed crops at plot scale in temperate areas using the joint use of optical (Sentinel-2), radar (Sentinel-1) and meteorological (SAFRAN) data. The novelty comes from the combined use of vegetation, polarisation and meteorological indices. The study area is located in southwest France, and the summer crops to be classified are maize (both irrigated and rainfed), soybean (both irrigated and rainfed) and sunflower (rainfed). As only part of the summer crops was irrigated in the study area, one challenging point was to distinguish between irrigated and rainfed plots of the same species. In order to make this discrimination, we relied on the phenological development of the vegetation cover as a explanatory variable. Different scenarios were used to evaluate the performance of classifications models as a function of the various types and number of features. Different scenarios were evaluated using ground truth data collected in 2017 and 2018. These two years were characterised by contrasted meteorological conditions, which allowed to analyse the performance of the method under various climatic conditions.

2. Study Site and Dataset

The study site is a watershed (Adour Amont) located in the southwestern France, west of Toulouse (city). It covers 1500 km^2, as shown in Figure 1. The climate is temperate with continental and oceanic influences. It is characterised by a hot summer (mean T° = 22 °C) and a wet spring (mean rainfall = 108 mm) [40]. In this region, the minimum rainfall occurs between July and October, which corresponds to the maximum development of summer crops, as shown in Table 1, making irrigation mandatory. Maize, soybean and sunflower represent, respectively, 82%, 9% and 8% of the summer crops, i.e., 36% of the whole cultivated crops, according to the agricultural Land Parcel Information System "Registre Parcellaire Graphique" (RPG) provided by the French Services and Payments Agency [41]. The RPG contains information on crop types but no information on agricultural practices. Only maize and soybean are irrigated and the irrigation water needs represent 30 million m^3 over the season [42]. The two years studied are characterised by different weather conditions over the cropping period. The year 2017 can be defined as a dry year, as it has a total rainfall of 424 mm compared to 573 mm in 2018.

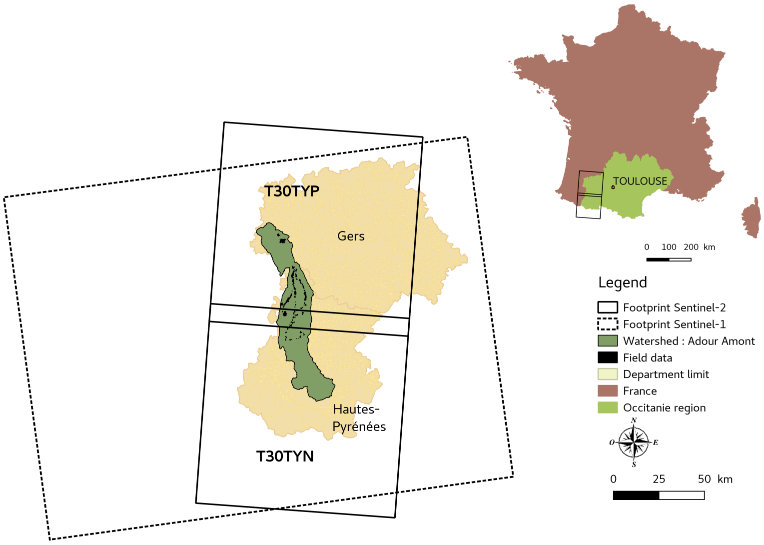

Figure 1. Location of the study area with footprints of the Sentinel-1, Sentinel-2 images and field data.

Table 1. Theoretical cropping calendar of the studied summer crops: the green squares illustrate the theoretical period when the crop is sown, and the brown squares illustrate the period when the crop is harvested.

	Growing Year											
	Jan.	**Feb.**	**Mar.**	**April**	**May**	**June**	**July**	**Aug.**	**Sept.**	**Oct.**	**Nov.**	**Dec.**
Maize				🟩	🟩				🟫	🟫	🟫	
Soybean				🟩	🟩				🟫	🟫		
Sunflower				🟩	🟩			🟫	🟫			

2.1. The Reference Dataset

The reference dataset was established from field campaigns carried out at two stages of the growing season: after sowing (May) and at flowering (July). The identification of the irrigation practices was based on the presence of irrigation equipment or through declarative information carried out by the farmer. The reference dataset consisted of 832 plots in 2017 (557 irrigated and 275 rainfed) and 942 plots in 2018 (680 irrigated and 262 rainfed) as shown the Table 2. Within the dataset, irrigated maize is the most represented crop with 60% of the plots sampled in 2017 and 48% in 2018. Irrigated soybean is the least represented crop in the dataset with 3% in 2017 and 5.6% of the plots sampled in 2018. This low sampling of irrigated and rainfed soybean is explained by the low representativeness of this crop in the territory (<10%), contrary to maize which represents 82% of the agricultural plots cultivated in summer crops in 2017 and 84% in 2018. Maize and soybean areas are increasing, while sunflower areas are decreasing between the two years, according to the RPG. The plots are located on gentle slopes (less than 5%) and on alluvial soil [43]. The dataset represented 21% of the total area of the summer crops in the territory.

Table 2. Distribution of reference dataset by class for 2017 and 2018.

Class Label	**Number of Plots**		**Total Area Sampled (ha)**		**Distribution (%)**		**RPG (%)**	
	2017	**2018**	**2017**	**2018**	**2017**	**2018**	**2017**	**2018**
Maize irrigated	526	639	943	727	60	48.1	82.8	84
Maize rainfed	198	175	302	500	19.2	33.1		
Soybean irrigated	31	41	54	85	3.4	5.6	8.2	9.6
Soybean rainfed	27	38	77	151	4.9	10		
Sunflower	50	49	120	40	7.6	2.7	8.6	5.5

2.2. Sentinel-2

The Sentinel-2 (S2A-S2B) images were processed to level 2A with the MAJA processing chain [44,45], allowing to obtain surface reflectances at top of canopy (TOC). This process presented in Hagolle et al. and Baetens et al. [44,45], allows the detection of clouds and their shadows, the correction of the atmospheric effects of the images from an estimation of the aerosol optical thickness (AOT) and water vapour. This process can be applied to time series of images. 100 images were processed in 2017 and 124 in 2018, corresponding to the tiles T30TYN and T30TYP, on Theia website [https://theia.cnes.fr/]. The average number of cloudy pixels was 31% in 2017 and 37% in 2018 over the whole time series, with cloudiness reaching over 85% in June (spring). The obtained images were temporally aggregated to regular 10-day interval composite datasets using the gapfilling module Orfeo Toolbox 6.7 (OTB) [46]. This temporal resampling relies on a distance-weighted linear interpolation of the clear acquisition dates of the optical satellites taking into account cloud and cloud shadow masks, which is necessary to study very large areas, as it limits the impact of satellite tracks, clouds and their shadows [28,47].

2.3. Sentinel-1

The Sentinel-1 images came from the C-SAR instrument onboard two Sentinel 1 satellites (S1A-S1B) (Interferometric Wide Swath mode, IWS-GRD [26]). This mode provides dual-polarisation (VV and VH) imagery, at resolution of 20 m, with a swath of 250 km. The images were radiometrically (Multilooking filter 2 × 2) and geometrically corrected using the OTB software [46]. Only Sentinel-1 images acquired in ascending mode (acquisition time: 6.00 pm) and between April and November were used (i.e., one image every 6 days, i.e., 79 images in 2017 and 100 in 2018). The ascending mode (orbit n°30) was used in the study, to limit the impact of morning dew and freezing dew, which can lead to artefacts in the SAR signal. Like Sentinel-2 images, the SAR images were orthorectified on the S2 grid and with the same pixel size. In addition to the orthorectification process, the SAR images were linearly interpolated every 10 days to maintain the same temporality in the satellite data between Sentinel-1 and Sentinel-2.

2.4. Meteorological Data

Rainfall data from the SAFRAN database [40] were used in the classification process. It is defined in mm/day. SAFRAN is a system for atmospheric analysis of surface meteorological variables based on the use of homogeneous climatic zones and capable of taking into account altitudinal variations. These data are spatially interpolated to cover all of mainland France with a regular grid of (8 × 8 km).

3. Methods

Figure 2 illustrates the methodology used. It includes 4 main steps: (1) preprocessing of the initial images, which enables the calculation of cumulative monthly indices from time series; (2) pixel classification based on cumulative monthly indices; (3) postprocessing of the classifications, with the aim of removing of isolated pixels; and (4) validation of the resulting maps.

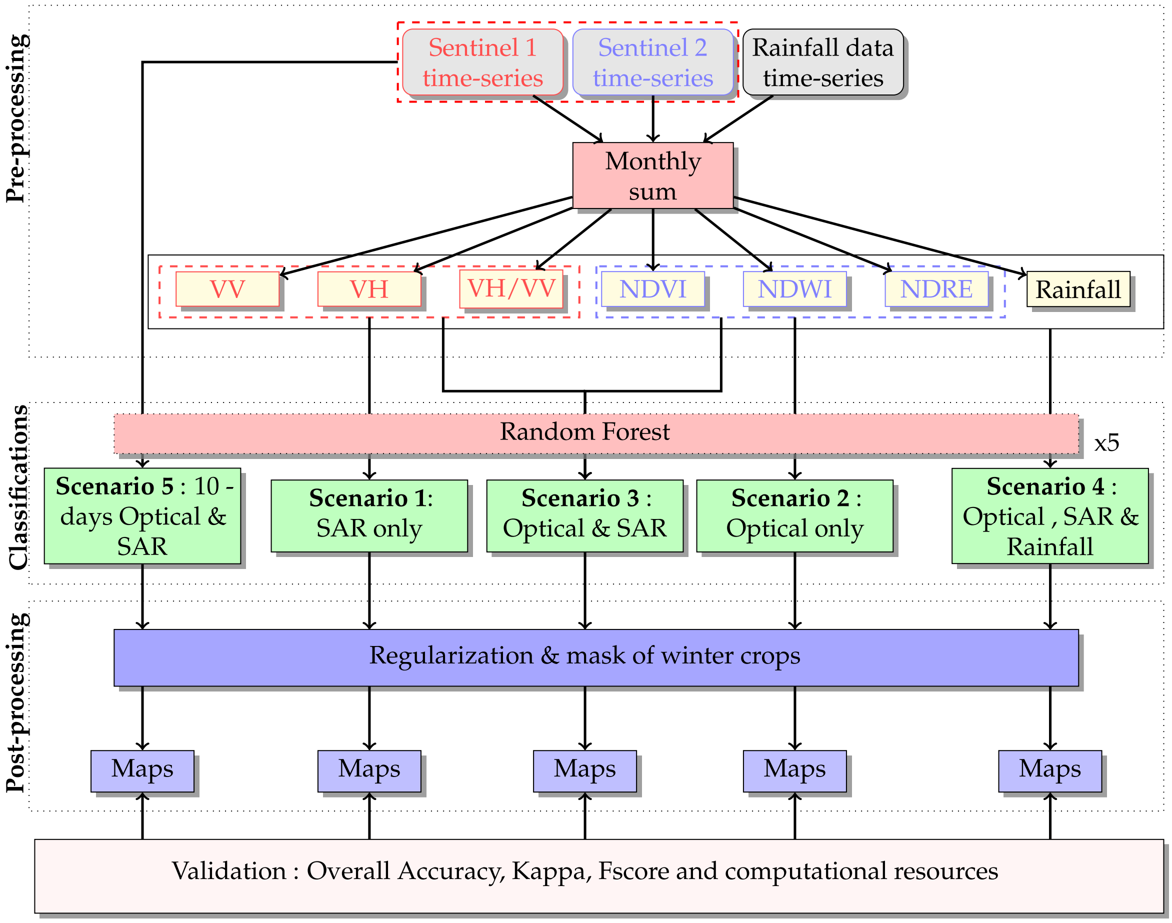

Figure 2. The workflow of the methodology used in this study. The grey squares represent the initial data. The yellow squares are the stacks of monthly cumulative indices after processing by the algorithm, represented by a red square. The green squares correspond to the different scenarios tested. The blue squares represent different maps from the classifiers, i.e., classifications and confidence maps.

3.1. Feature Computation

3.1.1. Optical Features

As shown on Table 3, the optical features involved into the classification process are the Normalized Difference Vegetation Index (NDVI), the Normalized Difference Red-Edge (NDRE) and the Normalized Difference Water Index (NDWI). These indices were selected as they are sensitive to various characteristics of the plants: the fraction of green vegetation cover [48,49], the foliar pigment [50,51] and the plant water content [52], respectively. Figure 3 illustrates the dynamics of vegetation cover growth between irrigated and rainfed crops. A significant difference is observed at full growth ($NDVI > 0.8$ and $NDWI < -0.40$) . This difference is stronger in 2017. It decreases when entering the senescent phase. The growing cycle is quite synchronous for all crops, as shown in the Table 1. For sunflowers, the growth cycle is different than for other crops, with lower growth peaks.

Table 3. Optical and radar features.

Name	Description	Equation
NDVI	Normalized Difference Vegetation Index	(NIR − Red)/(NIR + Red)
NDRE	Normalized Difference Red-Edge	(NIR − Red-Edge)/(NIR + Red-Edge)
NDWI	Normalized Difference Water Index	(NIR − SWIR)/(NIR + SWIR)
VV	Vertical—Vertical Polarisation	-
VH	Vertical—Horizontal Polarisation	-
VH/VV	Ratio	-

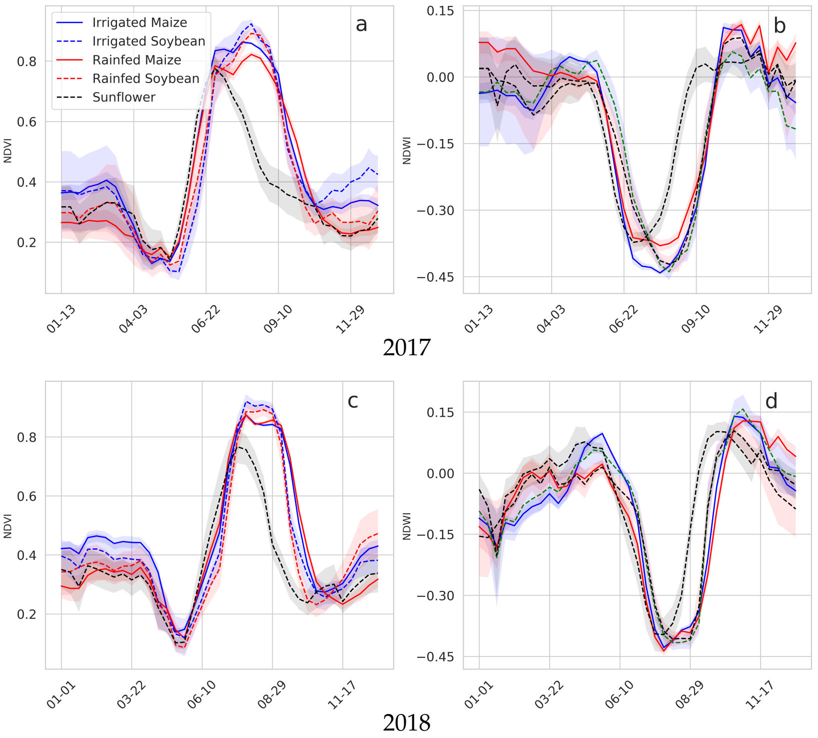

Figure 3. Dynamics of optical indices (Normalized Difference Vegetation Index (NDVI) (**a**,**c**) and Normalized Difference Water Index (NDWI) (**b**,**d**)) for maize, soybean and sunflower crops. The solid line curves represent maize, the dotted line represents soybean, with irrigated blue and rainfed red for both crops. The black curve represents sunflower. The envelope around the curves corresponds to the 95% confidence interval.

3.1.2. Radar Features

VV and VH polarisations were used into the classification. They are, respectively, sensitive to soil moisture [53–55] and to the volume scattering of vegetation [53,56]. As SAR backscatter time profiles in both polarisations are noisy by environmental factors , we used the VV/VH ratio which partially compensates these effects. The dynamics of SAR polarisations differ between rainfed and irrigated crops, as shown in Figure 4. This difference is more marked throughout the season than for optical indices. Moreover, there is a clear difference in the amplitude of the SAR signal between the two types of crops (soybean and maize) at full growth.

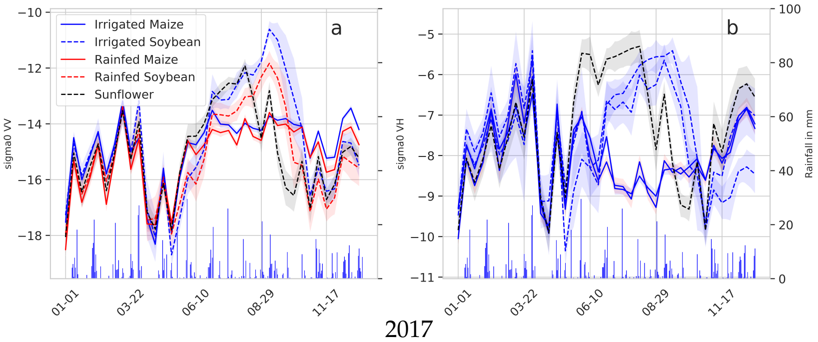

2017

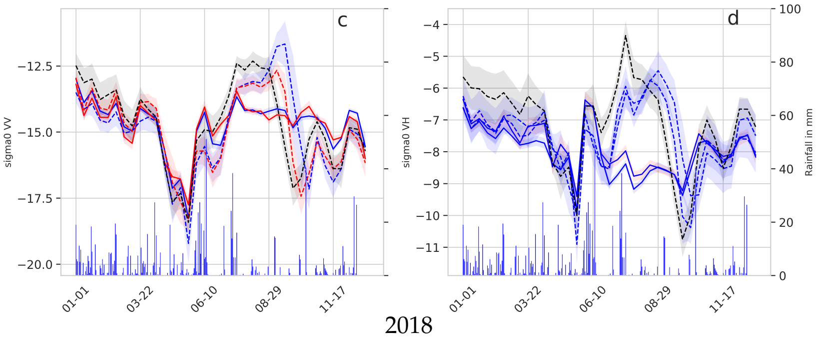

2018

Figure 4. Dynamics of SAR polarisations (VV (**a**,**c**) and VH (**b**,**d**)) for maize, soybean and sunflower crops, The solid line curves represent maize, the dotted line represents soybean, with irrigated blue and rainfed red for both crops. The black curve represents sunflower. The envelope around the curves corresponds to the 95% confidence interval.

3.1.3. Cumulative Indices

The use of multispectral (optical and radar) and multi-temporal images products leads to an increase in the number of features, to be processed, and consequently increase the redundancy of spectral information and the computation time of the classification process. To avoid these effect, we computed cumulative monthly indices, correspond to the sum of the spectral information of each feature (rainfall, optical and radar). We used gap filling for simplicity. The use of cumulative indices sounds pertinent as they are related to the plant functioning. Indeed, many authors have demonstrated the link between plant development of the plant and the cumulative spectral indices provided by remote sensing data [57–59]. For this study, we assumed that the irrigation have an impact of several irrigation events (4 to 5 irrigations) on crop development could be captured using the cumulative indices over the growing season. Indeed, we assume that the speed and amplitude of crop development differs between irrigated and non-irrigated crops at the end of the season.

3.2. *Classification*

The algorithm used for the classification process is the Random Forest (RF) [60]. It was selected for its robustness, because it is easier to parametrise and has good performances [29,30,61–64]. The Random Forest library used is the one provided by Shark [65] available through the supervised classification framework of Orfeo Toolbox 6.7 [46]. The number of trees was set to 100, the maximum depth to 25 and max-features to $\sqrt{number features}$.

The pixel classification procedure has been fully automated by the Iota2 processing chain developed by CESBio and available as free software [https://framagit.org/iota2-project/iota2.git]. Each classification was evaluated using the reference data set, which was randomly divided into two parts: 50% of the plots were used for the training phase and 50% were used for validation. This division into two parts avoids an optimistic estimate of the performance of the classification, as it ensures that correlated pixels from the same plot will not be used for training and validation This division into two parts is performed for each run. RF classifiers can perform poorly when the number of training pixels for each class is unbalanced. To address this problem, the maximum number of training pixels per class has been limited to 10,000. Limiting the maximum number of pixels also reduces the training time of the classifier. For those classes where fewer pixels were available, all the pixels in the training set were used. In our case, the soybean classes (irrigated and rainfed) had less than 10,000 training pixels because this crop is poorly represented in the territory.

3.3. Scenarios

Several scenarios were evaluated:

- Scenario 1: with monthly cumulative SAR features only (VH, VV, VH/VV) referenced as "SAR only" in Figure 2,
- Scenario 2: with monthly cumulative Sentinel 2 features only (NDVI, NDRE, NDWI) referenced as "Optical only" in Figure 2,
- Scenario 3: with monthly cumulative optical and SAR features referenced as "Optical and SAR" in Figure 2,
- Scenario 4: scenario 3 with in addition cumulative rainfall referenced as "Optical, SAR and Rainfall" in Figure 2,
- Scenario 5: 10-day Optical, SAR features referenced as "10-day Optical and SAR" in Figure 2.

The total number of features over the entire study period of each scenario is given the Table 4.

Table 4. Summary of the different scenarios tested, with the number of features over the period from April to November.

	ID	Scenario	Number of Features
Cumulative	1	SAR only	24
	2	Optical only	24
	3	Optical and SAR	48
	4	Optical, SAR and rainfall data	56
Not cumulative	5	10-day Optical and SAR	385

3.4. Validation

Each metric was averaged over the five runs to obtain a mean value and a confidence interval per scenario and to measure robustness against the sample selection noise. The global performance was evaluated using the Kappa coefficient (1) and the Overall Accuracy (OA). The Kappa coefficient expresses a relative difference between the observed agreement Po and the random agreement which can be expected if the classifier was random, Pe. The Overall Accuracy (OA), is the total number of correctly classified pixels divided by the total number of validation pixels.

$$Kappa = \frac{P_o - P_e}{1 - P_e} \tag{1}$$

with $P_o = \frac{1}{n}\sum_{i=1}^{r} n_{ii}$ and $P_e = \frac{1}{n^2}\sum_{i=1}^{r} n_i n_i$, The performance of the different scenarios was evaluated using the reference datasets. Table 5 shows the number of pixels used for learning and validation of the classification model for each class. In view of the strong imbalance between the two datasets (Training and Validation), we know that the overall accuracy may be biased by the majority classes. To limit this bias, we decided to use another metric at the class level.

The performance of each class was evaluated using the Fscore (2).

$$Fscore = 2 \times \frac{Accuracy \times Recall}{Accuracy + Recall} \tag{2}$$

where

- Accuracy is the ratio between the correctly classified pixels and the sum of all pixels classified as this class, and
- Recall is the ratio between the correctly classified pixels and the total number of reference data pixels of that class.

The central processing unit (CPU) time and allocated Random Access Memory (RAM) were also analysed in order to define a trade-off between classifier performance and use of computational resources. This evaluation was carried out for the two steps of the classification process: the model learning and the classification steps.

Table 5. Number of pixels for learning and validation of the model, for each class and for each year.

Class Label	**2017**		**2018**	
	Training	**Validation**	**Training**	**Validation**
Irrigated Maize	10,000	51,731	10,000	33,651
Rainfed Maize	10,000	12,606	10,000	24,899
Irrigated Soybean	3388	2173	3844	4973
Rainfed Soybean	3461	4437	7319	7464
Sunflower	6502	4853	2173	1662

3.5. Confidence Map

The map of irrigated areas contains for each pixel the label selected by the classifier, which is a majority vote on the labels selected by all the decision trees in the forest. The probability of each class can be estimated as the proportion of trees in the forest that chose that label. It is therefore possible to associate a confidence to the decision using the probability of the majority class. Although this confidence estimate may be valuable to the user, it should be kept in mind that it is an estimate of the classifier itself, and may therefore be erroneous. The correlation between confidence and classification quality was assessed by Inglada et al. [47].

3.6. Postprocessing

A regularisation was applied to the final classification in order to remove isolated pixels. This procedure filters the input labelled image using majority vote in a 3 × 3 neighbourhood. The majority vote takes the most representative value of all identified pixels and then sets the centre pixel to this majority label value [46]. The winter crops were also masked using the RPG of the classified year.

4. Results

4.1. Performance of Each Scenario

The global performances of the classifications are shown in Figure 5. The best results are obtained with the 10-days scenario 5.

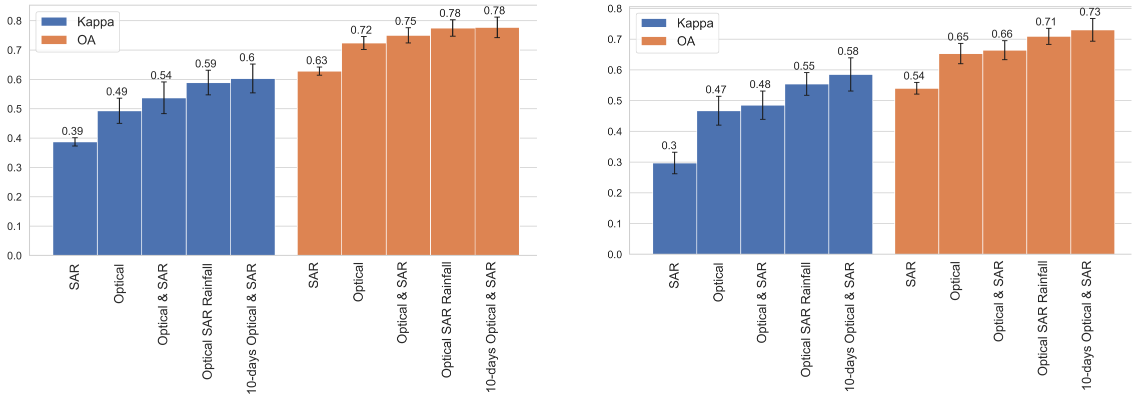

(**a**) 2017 (**b**) 2018

Figure 5. Performance for each scenarios.The orange and blue bars correspond to Overall accuracy and Kappa respectively. (**a**) illustrates the results obtained in 2017 and (**b**) corresponds to those obtained in 2018.

The classifications with cumulative indices lead to performances slightly inferior to the 10-days classifications (OA = 0.78 in 2017), while significantly reducing the RAM usage and CPU time, as shown in the Table 6. RAM is reduced by a factor of 2 for the learning phase. The CPU time is reduced by a factor of 2 for the learning step and by a factor of 4 for the classification step. Therefore, scenario 4 may be considered a good trade-off between accuracy and computational resources. However, we should note that Kappa values (≈0.6) are quite low even for the best configuration. For the further analysis, we retained the scenarios combining optical and radar features (scenarios 3, 4 and 5) as were supposed to be more robust to various meteorological conditions.

Table 6. Computational resources for the learning and classification stages, for each scenario.

			CPU Time (in Hours)		RAM (in GB)	
Scenario	**ID**	**Nb. of Features**	**Model Learning**	**Classification**	**Model Learning**	**Classification**
SAR	1	24	4.5	176	0.21	19
Optical	2	24	2.2	150	0.14	19
Optical & SAR	3	48	4.5	181	0.23	21
Optical SAR and Rainfall	4	54	3.5	164	0.22	21
10-days Optical & SAR	5	385	6.6	739	0.57	22

4.2. Fscore Results

Figure 6 shows the Fscores for the three scenarios. The best performances are observed for sunflower for both years (Fscore > 0.9), irrigated maize in 2017 (Fscore > 0.85) and irrigated soybean in 2018 (Fscore > 0.68). The lowest scores are observed for the irrigated soybean in 2017 (0.28 < Fscore < 0.4). Intermediate Fscore (0.4 to 0.8) are observed for the rainfed maize and rainfed soybean.The same trends are observed for all scenarios.

Except for sunflower, adding rainfall into the cumulative method (Scenarios 3 and 4) improves the Fscore and allows to reach performance comparable to the 10-day scenario (Scenario 5).

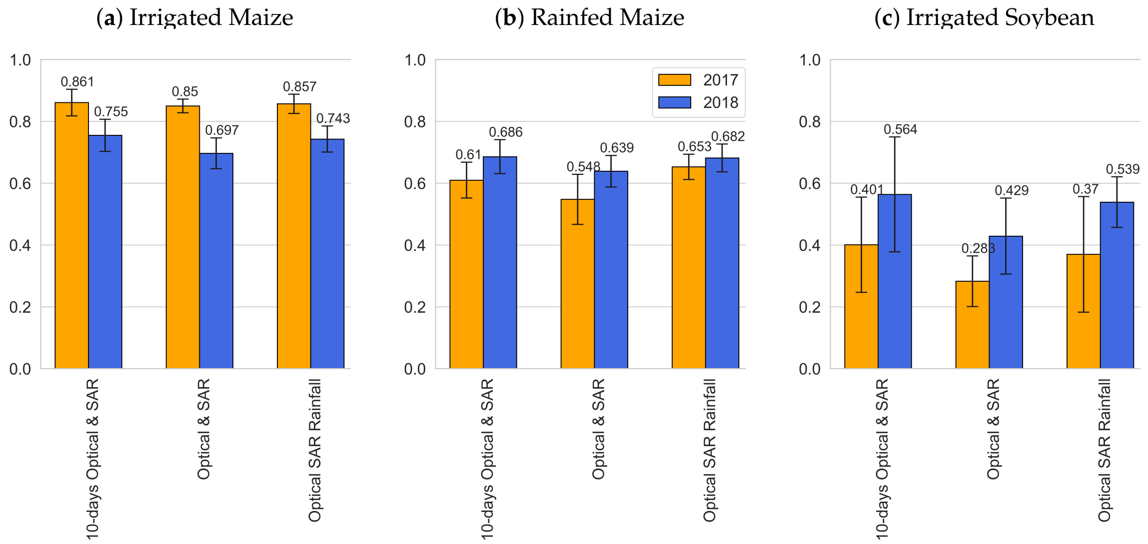

(**a**) Irrigated Maize (**b**) Rainfed Maize (**c**) Irrigated Soybean

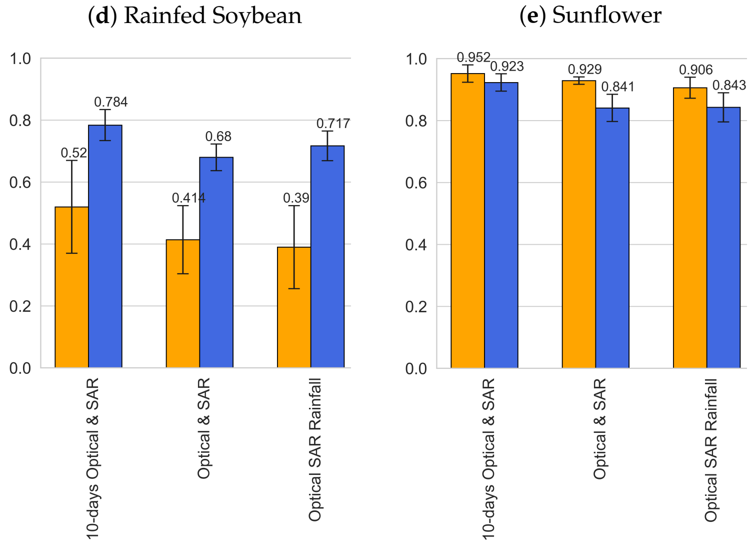

(**d**) Rainfed Soybean (**e**) Sunflower

Figure 6. Fscore by class as a function of the 3 scenarios. The orange and blue bars correspond, respectively, to the years 2017 and 2018.

4.3. Analysis of Confusion Between Classes for Irrigated Crops

The confusion between classes were analysed for the three scenarios. Figure 7 illustrates the percentage of confusion between classes for both years, i.e., the percentage of prediction error.

For both years and regardless of the scenario, confusion are observed between practices (irrigated and rainfed) for a given crop but little confusion occurs between crops. The strongest confusions (30% < Fscore < 50%) are observed in 2017 between irrigated and rainfed soybean (Figure 7b,d) as observed on the Fscore values (Figure 6). Lowest confusions are observed between irrigated and rainfed maize, for both years, with Fscore values varying from 10 to 30%, in average (Figure 7a,c).

Moreover, the use of rainfall data allows for a reduction in confusions for all classes. Indeed, the percentages of confusions are almost systematically lower for scenario 4 compared to those obtained for scenario 3.

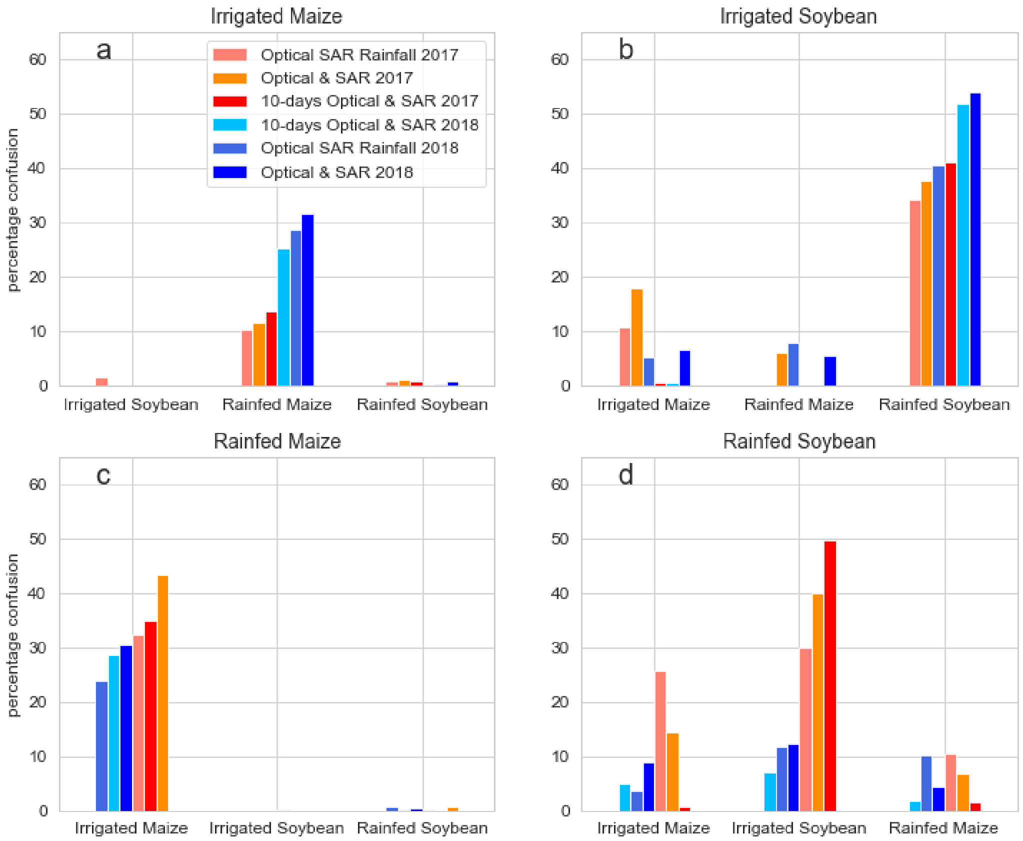

Figure 7. Confusion according to the scenarios. The title of each sub-graph corresponds to the real class and the labels in the horizontal axis refer to the predicted classes. The letter on each graph corresponds to a crop, with (**a**): irrigated maize, (**b**): irrigated soybean, (**c**): rainfed maize and (**d**): rainfed soybean.

4.4. Confidence Map

Figure 8 shows the confidence index for each pixel on scenarios 3 (Figure 8a) and 4 (Figure 8b) in 2017. The best confidence for all classes combined is for scenario 4 for both years. Indeed, the average confidence is 69.5% ± 8% for scenario 4 compared to 63% ± 10% for scenario 3 in 2017 and 63% ± 10% and 72.10% ± 7% for scenarios 3 and 4, respectively, in 2018. We also see in Figure 8 that some areas, such as the Northeast, still have low confidence despite the addition of rainfall. These areas remain difficult to classify by the model. The Table 7 shows the average percentage of confidence for each class. Irrigated and rainfed maize and sunflower have the highest confidence for both years. Irrigated and rainfed soybeans have the lowest confidence and those for both years studied.

Table 7. Average confidence for the years 2017 and 2018, with associated standard deviations, expressed in %.

Class Label	**2017**		**2018**	
	Scenario 3	**Scenario 4**	**Scenario 3**	**Scenario 4**
Irrigated maize	73 ± 10	84 ± 8	70 ± 10	84 ± 7
Rainfed maize	70 ± 11	78 ± 9	62 ± 10	72 ± 11
Irrigated soybean	55 ± 11	61 ± 11	64 ± 12	65 ± 12
Rainfed soybean	53 ± 12	62 ± 14	56 ± 11	59 ± 9
Sunflower	89 ± 8	92 ± 4	56 ± 13	74 ± 12

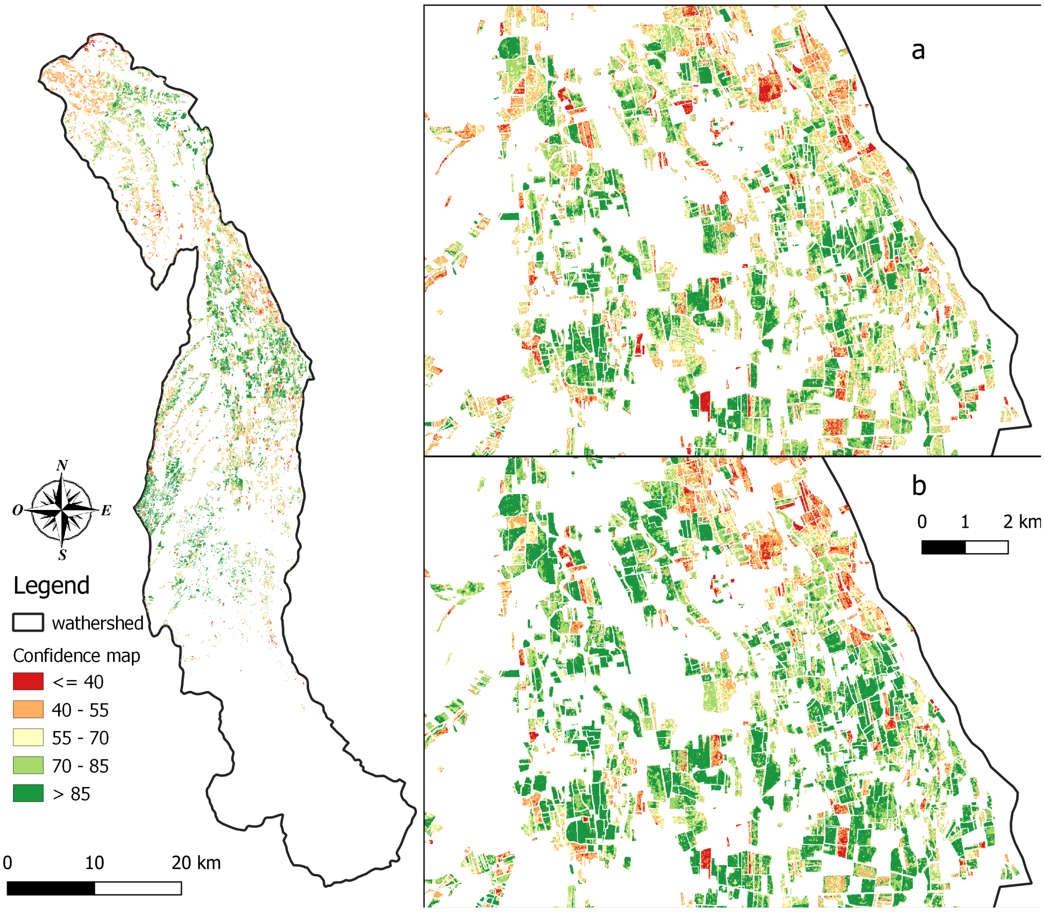

Figure 8. Confidence map for 2017: (**a**) scenario 3 and (**b**) scenario 4.

4.5. Regional Statistics

Table 8 shows the total areas by crop provided by scenario 4 and 5 and compared to RPG for the entire study area. The areas estimated were similar to the RPG, with average errors per class not exceeding ±8% for Scenario 5. However, the errors were higher for Scenario 4. Maize is the crop with the best area estimated by both scenarios, with an average error of ±2%. In contrast, soybeans have an average error of ±15%, with the largest gap observed in 2017 in Scenario 4. Scenario 5 produced to better performances.

Table 8. Summary of areas by class for Scenarios 4 and 5 and the RPG for the years 2017 and 2018. They are expressed in hectares. The term diff. refers to the difference between the area from the scenario and the RPG. It is expressed as a percentage.

Class Label			**2017**					**2018**		
	RPG	**Scenario 4**	**Diff.**	**Scenario 5**	**Diff.**	**RPG**	**Scenario 4**	**Diff.**	**Scenario 5**	**Diff.**
Maize	20,987	21,479	+2%	20,601	−2%	20,242	20,695	+2%	20,149	−1%
Sunflower	2210	1973	−11%	2183	−1%	1242	1131	−9%	1339	+8%
Soybean	2301	1402	−39%	2445	+6%	2326	2001	+2%	2339	0%
Total	25,498	24,854	−3%	25,229	−1%	23,811	23,827	0%	23,827	0%

5. Discussion

5.1. Optical or/and Radar Features

Scenarios 1 and 2, based on single-source use of radiometric information, show the worst performance in terms of OA and Kappa coefficient (between 0.3 and 0.49). The low Fscore obtained with the radar data only is due to the large variations in the SAR signal and the lack of spectral information that does not allow good discrimination between classes. Indeed, SAR polarisations are the result of multiple contributions, between rain, vegetation and tillage, leading to classification errors. The results obtained by this scenario are in agreement with those obtained by Ferrant et al., on the Telangana province in South India with a Kappa coefficient between 0.3 and 0.49 depending on the year [35]. The poor performance of scenario 2 is due to the low number of features, caused by cloud cover (37% in 2017 and 31% in 2018), and the absence of the 2B sensor in 2017 that can make crop growth detection difficult like frequently observed in [9,10,33,35,36].

Thus so-called "single-source" scenarios are highly dependent on the number and quality of the dataset. Figure 5 reveals that the synergy optical and radar data permits to limit the impact of cloud cover, with a gain in all metrics for both years. Similar results were found in the literature with a significant gain in performance on the detection of irrigated areas in India (more than 74% gain on the Fscore and 0.20 on the kappa coefficient, when the synergy of the two sensors is used) [35], in Northern Spain, with a 5% increase in overall accuracy compared to using Sentinel-1 data alone [37].

5.2. Impact of Cumulative Indices

Dealing with the huge number of images available requires optimised computing methods. To avoid this constraint, we evaluated the performance of classifications with a reduced number of indices. Results show that cumulative indices lead to similar performances for maize (irrigated/rainfed) than the overall 10-day features (Figure 5), meaning that these is redundant information when using all the full spectral bands and dates. The lowest Fscore observed for the minority classes (Soybean and rainfed maize) is due to a deficit of learning samples. Indeed, the low number of reference dataset for theses classes does not allow to characterise the whole spatial and temporal variability of these classes, and consequently leads to a high degree of confusion, as shown in Figure 7. However, Scenario 5 is seems less sensitive to the size of reference dataset. The addition of the learning data for the soybean and rainfed maize in 2018, the results were improved with lower confusion (Figure 7) and higher Fscore. This link between performance of the classification methods and the number of reference data has been raise by Pelletier et al. [64]. For sunflowers, there is a decrease in Fscore and confidence between 2017 and 2018, which is explained by a smaller sample area in 2018, with only 40 ha, compared to 120 ha in 2017. Nevertheless, this small sample area does not have a significant impact on the results, as the phenology of this crop is very different from that of the other crops studied, as shown in Figure 3.

Much less computational resources was needed for the cumulative approach, as shown in Table 6. Classifications based on the use of cumulative indices (56 features) lead to similar performances to classifications using the 10-days features (385 features), while reducing the consumption of the computing resources by a factor of 4.

5.3. Contribution of Rainfall Features

The addition of rainfall data into the process slightly enhances the performance of the cumulative method, as illustrated by Fscore (Figure 6) and confidence (Section 4.4 and Table 7).

Indeed, adding these data improves the separability of the classes (Figure 7), and the possible noise of labelling present in the reference dataset. Nevertheless, they seem to lose importance during rainy years, as illustrated by the results on irrigated maize, which show a decrease in the Fscore between 2017 and 2018. This loss of efficiency can be explained by similar canopy growth dynamics between irrigated and rainfed crops, as rainfed crops are not subject to water stress limiting their phenological development during drought periods. These data also show that they can be used to discriminate rainfed and irrigated crops for near-real-time approaches [37]. Moreover, we note that scenario 4 is slightly faster compared to scenario 3 during the learning and application phase of the model (classification). This increase in speed is explained by the addition of rainfall data in the classification process which seems to simplify the choice of the classifier to assign a class to a given pixel.

The analysis of the confidence map illustrated in Section 4.4 confirms these results as the best confidence values are observed for scenario 4 (Figure 8) and those for both years. Nevertheless, the contribution of meteorological data does not significantly increase confidence for minority classes as shown in the Table 7. There are still areas where uncertainty remains high, as illustrated in the inserts of the Figure 8. As rainfall exhibits spatial heterogeneities all the ambiguities between irrigated and rainfed plots might not be removed. Indeed, the rainfall data used in our study have a low spatial resolution (8 km), which can increase confusions on the distinction between irrigated and rainfall.

6. Conclusions

The objective of this study was to establish a methodology for detecting irrigated and rainfed crops in temperate areas, using monthly cumulative of optical vegetation indices and SAR polarisations together. The use of these cumulative indices allows taking into account discrepancies on canopy development (speed and amplitude) between various crops and practices (irrigated and rainfed), while retaining all the spectral information. Classifications with radar only, or optical only, show poor performances (Kappa and OA < 0.5) caused by the lack of spectral information, not allowing a good discrimination of classes. The combined use of optical and radar features gives excellent results for irrigated maize (Fscore > 0.80), which represents 80% of the summer crops in the area. The results were worse for soybean (Fscore < 0.60), especially in 2017, which is explained by the lack of in situ reference data, partly due to the low representativeness of this crop on this territory (9%), making in situ collection difficult. In order to overcome this data constraint and to be able to extend the study area, the use of an eco-climatic spatial stratification could be envisaged as illustrated by Inglada et al. [47]. The use of spatial stratification would allow an improvement in performance as well as a better sampling of the minority classes.

In the course of this work, the contribution of rainfall data was also evaluated. The addition of these data allows a significant improvement of the Fscore for the irrigated and rainfed classes and a reduction of confusion between classes during dry years. However, the low spatial resolution of rainfall data used in our study (8 km), can lead to high uncertainties, especially in areas with strong rainfall heterogeneity. To limit these uncertainties, the use of data with a finer spatial resolution, like the AROME [66] or the COMEPHORE [67] data distributed by Météo-France, can be considered in a future work. Our study also reveals that the use of monthly cumulative indices leads to performances similar to those of the use of gap-filled images every 10 days while reducing the need of computer resources (×4). A cumulative method would seem to be the best choice for operational application, maintaining the best classification performances, while reducing the need of computational resources. The approach developed is valuable for cereal crops in temperate climate but it is might also be valuable for semi-arid areas where the contrasts between irrigated and rainfed crops are huge. However, that needs to be confirmed with further studies. The study could also be extended by an in-season study such as proposed in Demarez et al. [36] that revealed that the use of Landsat-8 and Sentinel-1 images allowed early detection of irrigated crops.

Author Contributions: Y.P. and V.D. conceived and designed the experiments; Y.P. conducted the experiments; Y.P., V.D., F.B. and J.I. analysed the results; Y.P. and V.D., wrote the article; J.I., N.B. and F.B. revised the paper. All authors have read and agreed to the published version of the manuscript.

Acknowledgments: This work is funded by the French space agency (CNES), Adour Garonne Water Agency and the Compagnie d'aménagement des coteaux de Gascogne, and it was carried out at the CESBIO laboratory. The authors would like to thank the Hautes Pyrénées Chamber of Agriculture for the data collection and T the development team of the iota^2 chain and especially Arthur Vincent for his help in the computer development of the method.

Conflicts of Interest: The authors declare no conflicts of interest.

References

1. Bruinsma, J. Food and Agriculture Organization of the United Nations. *World Agriculture: Towards 2015/2030: An FAO Perspective*; Earthscan Publications Ltd.: London, UK, 2003.
2. Schaldach, R.; Koch, J.; der Beek, T.A.; Kynast, E.; Flörke, M. Current and future irrigation water requirements in pan-Europe: An integrated analysis of socio-economic and climate scenarios. *Glob. Planet. Chang.* **2012**, *94*, 33–45. [CrossRef]
3. Dubois, O. *The State of the World's Land and Water Resources for Food and Agriculture: Managing Systems at Risk*; Earthscan Publications Ltd.: London, UK, 2011.
4. Ozdogan, M.; Yang, Y.; Allez, G.; Cervantes, C. Remote Sensing of Irrigated Agriculture: Opportunities and Challenges. *Remote Sens.* **2010**, *2*, 2274–2304. [CrossRef]
5. Bastiaanssen, W.G.; Molden, D.J.; Makin, I.W. Remote sensing for irrigated agriculture: Examples from research and possible applications. *Agric. Water Manag.* **2000**, *46*, 137–155. [CrossRef]
6. Bazzi, H.; Baghdadi, N.; El Hajj, M.; Zribi, M. Potential of Sentinel-1 Surface Soil Moisture Product for Detecting Heavy Rainfall in the South of France. *Sensors* **2019**, *19*, 802. [CrossRef]
7. Boken, V.K.; Hoogenboom, G.; Kogan, F.N.; Hook, J.E.; Thomas, D.L.; Harrison, K.A. Potential of using NOAA-AVHRR data for estimating irrigated area to help solve an inter-state water dispute. *Int. J. Remote Sens.* **2004**, *25*, 2277–2286. [CrossRef]
8. Kamthonkiat, D.; Honda, K.; Turral, H.; Tripathi, N.; Wuwongse, V. Discrimination of irrigated and rainfed rice in a tropical agricultural system using SPOT VEGETATION NDVI and rainfall data. *Int. J. Remote Sens.* **2005**, *26*, 2527–2547. [CrossRef]
9. Thenkabail, P.S.; Schull, M.; Turral, H. Ganges and Indus river basin land use/land cover (LULC) and irrigated area mapping using continuous streams of MODIS data. *Remote Sens. Environ.* **2005**, *95*, 317–341. [CrossRef]
10. Ozdogan, M.; Gutman, G. A new methodology to map irrigated areas using multi-temporal MODIS and ancillary data: An application example in the continental US. *Remote Sens. Environ.* **2008**, *112*, 3520–3537. [CrossRef]
11. Portmann, F.T.; Siebert, S.; Döll, P. MIRCA2000—Global monthly irrigated and rainfed crop areas around the year 2000: A new high-resolution data set for agricultural and hydrological modeling. *Glob. Biogeochem. Cycles* **2010**, *24*. [CrossRef]
12. Pervez, M.S.; Brown, J.F. Mapping irrigated lands at 250-m scale by merging MODIS data and national agricultural statistics. *Remote Sens.* **2010**, *2*, 2388–2412. [CrossRef]
13. Hajj, M.E.; Baghdadi, N.; Belaud, G.; Zribi, M.; Cheviron, B.; Courault, D.; Hagolle, O.; Charron, F. Irrigated Grassland Monitoring Using a Time Series of TerraSAR-X and COSMO-SkyMed X-Band SAR Data. *Remote Sens.* **2014**, *6*, 10002–10032. [CrossRef]
14. Zohaib, M.; Kim, H.; Choi, M. Detecting global irrigated areas by using satellite and reanalysis products. *Sci. Total Environ.* **2019**, *677*, 679–691. [CrossRef] [PubMed]
15. Thenkabail, P.; Dheeravath, V.; Biradar, C.; Gangalakunta, O.R.; Noojipady, P.; Gurappa, C.; Velpuri, M.; Gumma, M.; Li, Y.; Thenkabail, P.S.; et al. Irrigated Area Maps and Statistics of India Using Remote Sensing and National Statistics. *Remote Sens.* **2009**, *1*, 50–67. [CrossRef]
16. Cheema, M.J.M.; Bastiaanssen, W.G.M. Land use and land cover classification in the irrigated Indus Basin using growth phenology information from satellite data to support water management analysis. *Agric. Water Manag.* **2010**, *97*, 1541–1552. [CrossRef]
17. Dheeravath, V.; Thenkabail, P.S.; Chandrakantha, G.; Noojipady, P.; Reddy, G.P.O.; Biradar, C.M.; Gumma, M.K.; Velpuri, M. Irrigated areas of India derived using MODIS 500 m time series for the years 2001–2003. *ISPRS J. Photogramm. Remote Sens.* **2010**, *65*, 42–59. [CrossRef]
18. Gumma, M.K.; Thenkabail, P.S.; Hideto, F.; Nelson, A.; Dheeravath, V.; Busia, D.; Rala, A. Mapping irrigated areas of Ghana using fusion of 30 m and 250 m resolution remote-sensing data. *Remote Sens.* **2011**, *3*, 816–835. [CrossRef]
19. Ambika, A.K.; Wardlow, B.; Mishra, V. Remotely sensed high resolution irrigated area mapping in India for 2000 to 2015. *Sci. Data* **2016**, *3*, 160118. [CrossRef]

20. Bousbih, S.; Zribi, M.; El Hajj, M.; Baghdadi, N.; Lili-Chabaane, Z.; Gao, Q.; Fanise, P. Soil moisture and irrigation mapping in A semi-arid region, based on the synergetic use of Sentinel-1 and Sentinel-2 data. *Remote Sens.* **2018**, *10*, 1953. [CrossRef]
21. Gao, Q.; Zribi, M.; Escorihuela, M.J.; Baghdadi, N.; Segui, P.Q. Irrigation Mapping Using Sentinel-1 Time Series at Field Scale. *Remote Sens.* **2018**, *10*, 1495. [CrossRef]
22. Jalilvand, E.; Tajrishy, M.; Hashemi, S.A.G.Z.; Brocca, L. Quantification of irrigation water using remote sensing of soil moisture in a semi-arid region. *Remote Sens. Environ.* **2019**, *231*, 111226. [CrossRef]
23. Xie, Y.; Lark, T.J.; Brown, J.F.; Gibbs, H.K. Mapping irrigated cropland extent across the conterminous United States at 30 m resolution using a semi-automatic training approach on Google Earth Engine. *ISPRS J. Photogramm. Remote Sens.* **2019**, *155*, 136–149. [CrossRef]
24. Peña-Arancibia, J.L.; McVicar, T.R.; Paydar, Z.; Li, L.; Guerschman, J.P.; Donohue, R.J.; Dutta, D.; Podger, G.M.; van Dijk, A.I.J.M.; Chiew, F.H.S. Dynamic identification of summer cropping irrigated areas in a large basin experiencing extreme climatic variability. *Remote Sens. Environ.* **2014**, *154*, 139–152. [CrossRef]
25. Shahriar Pervez, M.; Budde, M.; Rowland, J. Mapping irrigated areas in Afghanistan over the past decade using MODIS NDVI. *Remote Sens. Environ.* **2014**, *149*, 155–165. [CrossRef]
26. Torres, R.; Snoeij, P.; Geudtner, D.; Bibby, D.; Davidson, M.; Attema, E.; Potin, P.; Rommen, B.; Floury, N.; Brown, M.; et al. GMES Sentinel-1 mission. *Remote Sens. Environ.* **2012**, *120*, 9–24. [CrossRef]
27. Drusch, M.; Del Bello, U.; Carlier, S.; Colin, O.; Fernandez, V.; Gascon, F.; Hoersch, B.; Isola, C.; Laberinti, P.; Martimort, P.; et al. Sentinel-2: ESA's Optical High-Resolution Mission for GMES Operational Services. *Remote Sens. Environ.* **2012**, *120*, 25–36. [CrossRef]
28. Inglada, J.; Arias, M.; Tardy, B.; Hagolle, O.; Valero, S.; Morin, D.; Dedieu, G.; Sepulcre, G.; Bontemps, S.; Defourny, P.; et al. Assessment of an Operational System for Crop Type Map Production Using High Temporal and Spatial Resolution Satellite Optical Imagery. *Remote Sens.* **2015**, *7*, 12356–12379. [CrossRef]
29. Valero, S.; Morin, D.; Inglada, J.; Sepulcre, G.; Arias, M.; Hagolle, O.; Dedieu, G.; Bontemps, S.; Defourny, P.; Koetz, B.; et al. Production of a Dynamic Cropland Mask by Processing Remote Sensing Image Series at High Temporal and Spatial Resolutions. *Remote Sens.* **2016**, *8*, 55. [CrossRef]
30. Immitzer, M.; Vuolo, F.; Atzberger, C.; Immitzer, M.; Vuolo, F.; Atzberger, C. First Experience with Sentinel-2 Data for Crop and Tree Species Classifications in Central Europe. *Remote Sens.* **2016**, *8*, 166. [CrossRef]
31. Sonobe, R.; Yamaya, Y.; Tani, H.; Wang, X.; Kobayashi, N.; Mochizuki, K.I. Assessing the suitability of data from Sentinel-1A and 2A for crop classification. *GISci. Remote Sens.* **2017**, *54*, 918–938. [CrossRef]
32. Vuolo, F.; Neuwirth, M.; Immitzer, M.; Atzberger, C.; Ng, W.T. How much does multi-temporal Sentinel-2 data improve crop type classification? *Int. J. Appl. Earth Obs. Geoinf.* **2018**, *72*, 122–130. [CrossRef]
33. Vogels, M.F.; De Jong, S.M.; Sterk, G.; Douma, H.; Addink, E.A. Spatio-temporal patterns of smallholder irrigated agriculture in the horn of Africa using GEOBIA and Sentinel-2 imagery. *Remote Sens.* **2019**, *11*, 143. [CrossRef]
34. Fieuzal, R.; Duchemin, B.; Jarlan, L.; Zribi, M.; Baup, F.; Merlin, O.; Hagolle, O.; Garatuza-Payan, J. Combined use of optical and radar satellite data for the monitoring of irrigation and soil moisture of wheat crops. *Hydrol. Earth Syst. Sci.* **2011**, *15*, 1117–1129. [CrossRef]
35. Ferrant, S.; Selles, A.; Le Page, M.; Herrault, P.A.; Pelletier, C.; Al-Bitar, A.; Mermoz, S.; Gascoin, S.; Bouvet, A.; Saqalli, M.; et al. Detection of Irrigated Crops from Sentinel-1 and Sentinel-2 Data to Estimate Seasonal Groundwater Use in South India. *Remote Sens.* **2017**, *9*, 1119. [CrossRef]
36. Demarez, V.; Helen, F.; Marais-Sicre, C.; Baup, F. In-Season Mapping of Irrigated Crops Using Landsat 8 and Sentinel-1 Time Series. *Remote Sens.* **2019**, *11*, 118. [CrossRef]
37. Bazzi, H.; Baghdadi, N.; Ienco, D.; El Hajj, M.; Zribi, M.; Belhouchette, H.; Escorihuela, M.J.; Demarez, V. Mapping Irrigated Areas Using Sentinel-1 Time Series in Catalonia, Spain. *Remote Sens.* **2019**, *11*, 1836. [CrossRef]
38. Bazzi, H.; Baghdadi, N.; Fayad, I.; Zribi, M.; Belhouchette, H.; Demarez, V. Near Real-Time Irrigation Detection at Plot Scale Using Sentinel-1 Data. *Remote Sens.* **2020**, *12*, 1456. [CrossRef]
39. Le Page, M.; Jarlan, L.; El Hajj, M.M.; Zribi, M.; Baghdadi, N.; Boone, A. Potential for the Detection of Irrigation Events on Maize Plots Using Sentinel-1 Soil Moisture Products. *Remote Sens.* **2020**, *12*, 1621. [CrossRef]

40. Durand, Y.; Brun, E.; Merindol, L.; Guyomarc'h, G.; Lesaffre, B.; Martin, E. A meteorological estimation of relevant parameters for snow models. *Ann. Glaciol.* **1993**, *18*, 65–71. [CrossRef]
41. Cantelaube, P.; Carles, M. Le registre parcellaire graphique: Des données géographiques pour décrire la couverture du sol agricole. In *Le Cahier des Techniques de L'INRA*; INRA: Paris, France, 2014; pp. 58–64.
42. IRRIGADOUR, O.U. *Organisme Unique de Gestion Collective IRRIGADOUR, Rapport Annuel 2018*; Technical Report; Organisme Unique IRRIGADOUR : Paris, France, 2019.
43. Monod, B. *Carte Géologique Numérique à 1/250 000 de la Région Midi-Pyrénées*; Notice Technique -BRGM/RP-63650-FR; BRGM: Paris, France, 2014; p. 160.
44. Hagolle, O.; Huc, M.; Villa Pascual, D.; Dedieu, G. A multi-temporal and multi-spectral method to estimate aerosol optical thickness over land, for the atmospheric correction of FormoSat-2, LandSat, VENμS and Sentinel-2 images. *Remote Sens.* **2015**, *7*, 2668–2691. [CrossRef]
45. Baetens, L.; Desjardins, C.; Hagolle, O. Validation of Copernicus Sentinel-2 Cloud Masks Obtained from MAJA, Sen2Cor, and FMask Processors Using Reference Cloud Masks Generated with a Supervised Active Learning Procedure. *Remote Sens.* **2019**, *11*, 433. [CrossRef]
46. Grizonnet, M.; Michel, J.; Poughon, V.; Inglada, J.; Savinaud, M.; Cresson, R. Orfeo ToolBox: Open source processing of remote sensing images. *Open Geospat. Data Softw. Stand.* **2017**, *2*, 15. [CrossRef]
47. Inglada, J.; Vincent, A.; Arias, M.; Tardy, B.; Morin, D.; Rodes, I. Operational High Resolution Land Cover Map Production at the Country Scale Using Satellite Image Time Series. *Remote Sens.* **2017**, *9*, 95. [CrossRef]
48. Tucker, C.J. Red and photographic infrared linear combinations for monitoring vegetation. *Remote Sens. Environ.* **1979**, *8*, 127–150. [CrossRef]
49. Huete, A.; Didan, K.; Miura, T.; Rodriguez, E.P.; Gao, X.; Ferreira, L.G. Overview of the radiometric and biophysical performance of the MODIS vegetation indices. *Remote Sens. Environ.* **2002**, *83*, 195–213. [CrossRef]
50. Gitelson, A.; Merzlyak, M.N. Spectral reflectance changes associated with autumn senescence of Aesculus hippocastanum L. and Acer platanoides L. leaves. Spectral features and relation to chlorophyll estimation. *J. Plant Physiol.* **1994**, *143*, 286–292. [CrossRef]
51. Sims, D.A.; Gamon, J.A. Relationships between leaf pigment content and spectral reflectance across a wide range of species, leaf structures and developmental stages. *Remote Sens. Environ.* **2002**, *81*, 337–354. [CrossRef]
52. Gao, B.C. NDWI—A normalized difference water index for remote sensing of vegetation liquid water from space. *Remote Sens. Environ.* **1996**, *58*, 257–266. [CrossRef]
53. Patel, P.; Srivastava, H.S.; Panigrahy, S.; Parihar, J.S. Comparative evaluation of the sensitivity of multi-polarized multi-frequency SAR backscatter to plant density. *Int. J. Remote Sens.* **2006**, *27*, 293–305. [CrossRef]
54. Jacome, A.; Bernier, M.; Chokmani, K.; Gauthier, Y.; Poulin, J.; De Sève, D. Monitoring volumetric surface soil moisture content at the La Grande basin boreal wetland by radar multi polarization data. *Remote Sens.* **2013**, *5*, 4919–4941. [CrossRef]
55. Amazirh, A.; Merlin, O.; Er-Raki, S.; Gao, Q.; Rivalland, V.; Malbeteau, Y.; Khabba, S.; Escorihuela, M.J. Retrieving surface soil moisture at high spatio-temporal resolution from a synergy between Sentinel-1 radar and Landsat thermal data: A study case over bare soil. *Remote Sens. Environ.* **2018**, *211*, 321–337. [CrossRef]
56. Chauhan, S.; Srivastava, H.S. Comparative evaluation of the sensitivity of multi-polarized SAR and optical data for various land cover classes. *Int. J. Adv. Remote Sens. GIS Geogr.* **2016**, *4*, 1–14.
57. Keeling, C.; Tucker, C.; Asrar, G.; Nemani, R. Increased plant growth in the northern high latitudes from 1981 to 1991. *Nature* **1997**, *386*, 698–702.
58. Dong, J.; Kaufmann, R.K.; Myneni, R.B.; Tucker, C.J.; Kauppi, P.E.; Liski, J.; Buermann, W.; Alexeyev, V.; Hughes, M.K. Remote sensing estimates of boreal and temperate forest woody biomass: Carbon pools, sources, and sinks. *Remote Sens. Environ.* **2003**, *84*, 393–410. [CrossRef]
59. Myneni, R.; Williams, D. On the relationship between FAPAR and NDVI. *Remote Sens. Environ.* **1994**, *49*, 200–211. [CrossRef]
60. Breiman, L. Random Forests. *Mach. Learn.* **2001**, *45*, 5–32. [CrossRef]

61. Miao, X.; Heaton, J.S.; Zheng, S.; Charlet, D.A.; Liu, H. Applying tree-based ensemble algorithms to the classification of ecological zones using multi-temporal multi-source remote-sensing data. *Int. J. Remote Sens.* **2012**, *33*, 1823–1849. [CrossRef]
62. Rodriguez-Galiano, V.F.; Ghimire, B.; Rogan, J.; Chica-Olmo, M.; Rigol-Sanchez, J.P. An assessment of the effectiveness of a random forest classifier for land-cover classification. *ISPRS J. Photogramm. Remote Sens.* **2012**, *67*, 93–104. [CrossRef]
63. Pelletier, C.; Valero, S.; Inglada, J.; Champion, N.; Dedieu, G. Assessing the robustness of Random Forests to map land cover with high resolution satellite image time series over large areas. *Remote Sens. Environ.* **2016**, *187*, 156–168. [CrossRef]
64. Pelletier, C.; Valero, S.; Inglada, J.; Champion, N.; Marais Sicre, C.; Dedieu, G. Effect of Training Class Label Noise on Classification Performances for Land Cover Mapping with Satellite Image Time Series. *Remote Sens.* **2017**, *9*, 173. [CrossRef]
65. Igel, C.; Heidrich-Meisner, V.; Glasmachers, T. Shark. *J. Mach. Learn. Res.* **2008**, *9*, 993–996.
66. Bouttier, F. Arome, avenir de la prévision régionale. In *La Météorologie*; Société Météorologique de France: Paris, France, 2007.
67. Tabary, P.; Desplats, J.; Do Khac, K.; Eideliman, F.; Gueguen, C.; Heinrich, J.C. The New French Operational Radar Rainfall Product. Part II: Validation. *Weather Forecast.* **2007**, *22*, 409–427. [CrossRef]